11-2017

Structural variations in the dithiadiazolyl radicals p-ROC6F4CNSSN (R = Me, Et, nPr, nBu): A case study of reversible and irreversible phase transitions in p-EtOC6F4CNSSN

Yassine Beldjoudi
University of Windsor

Rui Sun
University of Windsor

Ana Arauzo
Aragón Materials Science Institute

Javier Campo
Aragón Materials Science Institute

Robert J. Less
The University of Cambridge

See next page for additional authors

Published version can be found at: http://pubs.acs.org/doi/10.1021/acs.cgd.7b01065

Structural variations in the dithiadiazolyl radicals *p*-ROC$_6$F$_4$CNSSN (R = Me, Et, ^{n}Pr, ^{n}Bu): A case study of reversible and irreversible phase transitions in *p*-EtOC$_6$F$_4$CNSSN.

Yassine Beldjoudi,[a] Rui Sun,[a] Ana Arauzo,[b] Javier Campo,[b] Robert J. Less[c] and Jeremy M. Rawson[a,c]*

[a] Department of Chemistry & Biochemistry, University of Windsor, 401 Sunset Avenue, Windsor, ON, N9B 3P4, Canada. E-mail: jmrawson@uwindsor.ca

[b] Aragón Materials Science Institute (CSIC-University of Zaragoza) and Condensed Matter Physics Department, Facultad de Ciencias, E-50009 Zaragoza, Spain.

[c] Department of Chemistry, The University of Cambridge, Lensfield Road, Cambridge, UK CB2 1EW

ABSTRACT: The 4'-alkoxy-tetrafluorophenyl dithiadiazolyls, ROC$_6$F$_4$CNSSN [R = Me (**1**), Et (**2**), ^{n}Pr (**3**), ^{n}Bu(**4**)] all adopt *cis-oid* dimers in the solid state. The methoxy derivative **1** adopts a π-stacked AA'AA' motif whereas propoxy (**3**) and butoxy (**4**) derivatives exhibit an AA'BB' stacking. The ethoxy derivative (**2**) is polymorphic. The α-phase (**2α**) adopts an AA'BB' motif comparable with **3** and **4**, whereas **2β** and **2γ** are reminiscent of **1** but combine a mixture of both monomers and dimers in the solid state. The structure of **2β** exhibits Z' = 6 with two dimers and two monomers in the asymmetric unit but undergoes a thermally-induced phase transition upon cooling below -25 °C to form **2γ** (Z' = 14) with six dimers and two monomers in the asymmetric unit. The transition is associated with both rotation and translation of the dithiadiazolyl ring. Detailed DSC and variable temperature PXRD studies coupled with SQUID magnetometry have been used to show that **2α** converts irreversibly to **2β** upon heating and that **2β** and **2γ** interconvert through a reversible phase transition with a small thermal hysteresis in its magnetic response.

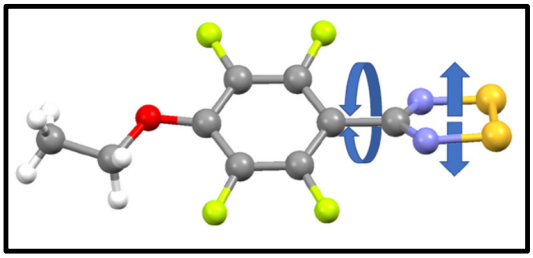

INTRODUCTION

Over the last 30 years 1,2,3,5-dithiadiazolyl (DTDA) radicals have been explored as building blocks for neutral radical conductors,[1] as building blocks in the design of some of the highest T_C organic magnets[2] and as components in photo-conducting devices.[3] They have also been used as ligands in coordination chemistry[4] and have been shown to undergo oxidative addition to low oxidation state metals.[5] More recent work has shown that poly-aromatic hydrocarbons bearing a DTDA moiety exhibit photoluminescence.[6]

The electronic properties of 1,2,3,5-dithiadiazolyl (DTDA) radicals such as conductivity and magnetism are heavily dependent on the solid-state structure.[7] Work by Rawson and Haynes identified common packing motifs between DTDA radicals in the absence of additional functionality (Scheme 1)[8] and the implementation of other strong structure-directing groups to dictate the structure have been reviewed.[9] The strong tendency of these radicals to dimerize (ΔH_{dim} ~ 35 kJ·mol^{-1})[10] has recently been used by Preuss as a supramolecular synthon for the self-organization of lanthanide-DTDA complexes.[11]

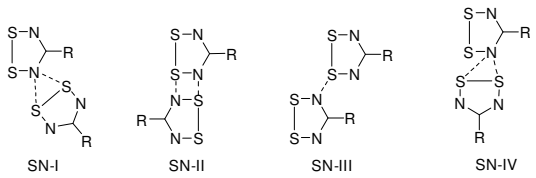

Scheme 1: Common favourable electrostatic in plane $S^{\delta+}...N^{\delta-}$ contacts identified in DTDA radicals.

The utilisation of DTDA radicals as building blocks for the design of organic magnetic materials necessitates that molecules retain their paramagnetic behavior.[7] Several strategies have been explored to potentially inhibit the dimerization process. While the presence of sterically demanding substituents can disrupt the common *cis-oid* dimerization (Scheme 2), alternative dimerization modes have been observed. The fine balance between monomer and dimer structures is exemplified by 2,4,6-(F$_3$C)$_3$C$_6$H$_2$CNSSN which was found to exist in both *trans-antarafacial* and monomeric forms.[12]

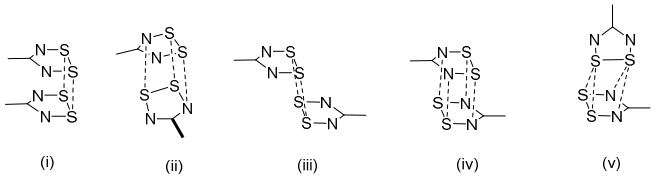

Scheme 2: Common dimerization modes of DTDA radicals: (i) *cis-oid*, (ii) *twisted*, (iii) *trans-antarafacial*, (iv) *trans-cofacial* and (v) *orthogonal* configurations.

The most commonly implemented approach to suppress dimerization has been the use of perfluoroaryl substituents coupled with structure-directing groups. In these cases, the electrostatic repulsion between the fluorines in the *ortho* position of the perfluoroaryl ring and the nitrogen of the heterocyclic ring leads to a large twist angle (energy minimum at $\theta \sim 50^{o}$)[13] between the two rings. This makes the perfluoroaryl ring sterically demanding, destabilizing the dimer. In the simplest case, 2,6-$F_2C_6H_3CNSSN$, the compound is found to be trimorphic with two *cis* dimers formed (tetragonal and monoclinic phases)[13] and a third monoclinic phase formed which comprises a *trans-antarafacial* dimer (Scheme 2) and a monomer,[14] reflecting the fine energetic balance between monomer and dimer in this system. In such cases, the inclusion of additional strong structure-directing groups may overcome the tendency for dimerization, exemplified by the presence of CN…S interactions in both α- and β-phases of *p*-NCC_6F_4CNSSN[15,16] as well as *p*-$NCC_6F_4C_6F_4CNSSN$.[17] Similarly NO_2…S interactions in *p*-$O_2NC_6F_4CNSSN$[18] and Br…N sigma-hole interactions in the case of *p*-BrC_6F_4CNSSN[19] appear adequate to overcome dimerization. In the current paper, we examine how subtle tuning of the 4'-substituent in the series *p*-ROC_6F_4CNSSN (R = Me, Et, ^{n}Pr and ^{n}Bu, Scheme 3) affects the solid-state structure and probe the polymorphic nature of **2**.

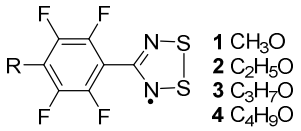

Scheme 3

RESULTS

All four 4-alkoxy perfluoroaryl carbonitrile derivatives, ROC_6F_4CN, were synthesized from a mixture of pentafluorobenzonitrile and sodium alkoxide in the corresponding alcohol based on the literature procedure (see ESI-2).[20] The 4'-alkoxy-functionalized perfluoroaryl DTDA radicals **1 – 4** were then prepared using standard synthetic methodologies[21] using triphenyl antimony as the reducing agent due to the low melting point of the radicals (60 – 80 °C) which avoided any contamination with Ph_3SbCl_2 (mp = 142 °C) during sublimation.[22] In this manner radicals **1 – 4** were obtained in crystalline form in 37 – 70 % recovered yield. Radical **2** was found to be polymorphic and careful monitoring of the temperature of the cold finger was required to selectively crystallize either **2α** or **2β**, a procedure that has been already utilised to selectively prepare α or β polymorphs of *p*-NCC_6F_4CNSSN.[15] In this fashion **2α** was selectively formed when collected on a cold-finger at -15 °C whereas **2β** was isolated when the 'cold' finger temperature was maintained at +30 °C. Polymorph **2γ** was formed through a solid state phase transition by cooling **2β** below -25 °C.

Crystal structures

Crystallographic data for **1** – **4** are summarized in Table 1. Radicals **1**, **3** and **4** adopt a single crystalline phase, whereas **2** crystallizes in three different phases; **2α**, **2β** and **2γ**.

Table 1: Crystallographic data for **1 – 4**

	1	**3**	**4**
Formula	$C_8H_3OF_4N_2S_2$	$C_{10}H_7OF_4N_2S_2$	$C_{11}H_9OF_4N_2S_2$
FW	283.24	311.3	325.3
Temp. (K)	150(2)	173(2)	173(2)
Crystal system	Monoclinic	Monoclinic	Monoclinic
Space group	$P2_1/c$	$P2_1/c$	$P2_1/c$
a/Å	7.3635(4)	16.2391(10)	16.9314(7)
b/Å	31.7443(17)	18.0475(9)	8.0672(3)
c/Å	8.3990(4)	8.1473(5)	22.8387(8)
α/°	90.00	90.00	90.00
β/°	101.436(2)	100.045(2)	124.995(2)
γ/°	90.00	90.00	90.00
V/Å^3	1922.28(17)	2351.2(2)	2555.51(17)
Z	8	8	8
D_c/g·cm^{-3}	1.955	1.759	1.691
R_{int}	0.040	0.055	0.046
R_1	0.051	0.047	0.043
wR_2	0.123	0.103	0.099
S	1.15	1.06	1.05
$\Delta\rho_{max}$, $\Delta\rho_{min}$ (e Å^{-3})	0.42, -0.54	0.45, -0.38	0.49, -0.39
	2α	**2β**	**2γ**
Formula	$C_9H_5OF_4N_2S_2$	$C_9H_5OF_4N_2S_2$	$C_9H_5OF_4N_2S_2$
FW	297.27	297.27	297.27
Temp. (K)	173(2)	253(2)	173(2)
Crystal system	Monoclinic	Triclinic	Triclinic
Space group	$P2_1/c$	*P*-1	*P*-1
a/Å	15.6073(15)	8.3271(8)	8.4511(15)
b/Å	17.3379(15)	11.9249(12)	25.774(4)
c/Å	8.1387(7)	35.154(4)	34.955(6)
α/°	90.00	94.5571(7)	90.013(4)
β/°	99.208(5)	91.851(6)	90.207(5)
γ/°	90.00	106.655(6)	94.726(5)
V/Å^3	2173.9(3)	3328.1(6)	7588(2)
Z	8	12	28
D_c/g·cm^{-3}	1.817	1.780	1.822
R_{int}	0.073	0.049	0.096
R_1	0.077	0.087	0.130
wR_2	0.170	0.245	0.341
S	1.11	1.02	1.04
$\Delta\rho_{max}$, $\Delta\rho_{min}$ (e Å^{-3})	0.50, -0.45	1.04, -0.45	1.21, -0.80

Selected structure parameters for **1 – 4** are reported in Table 2.

Crystal structure of 1

Radical **1** crystallises in the space group $P2_1/c$ with one *cis-oid* dimer (two crystallographically independent molecules) in the asymmetric unit. The twist angles between the heterocyclic ring plane and the aryl ring plane for the two molecules are 31.2(5)° and 30.8(5)°, comparable with other perfluorinated aryl DTDA radicals (14.5 – 57.8°, mean 37.8°).[16-19,23] Previous computational studies revealed an energy minimum at ~50° but a relatively shallow potential well for deviation away from this minimum such that angles in the range 30 to 90° fall within 3 kJ·mol^{-1} of this minimum.[13] A comparison of the experimentally observed torsion angles for fluorinated and non-fluorinated aryl groups in relation to the computed energies are presented in Fig. S.4.

The intra-dimer S···S contacts of 3.179(2) and 3.198(2) Å are significantly less than the van der Waals radii (3.60 Å), whereas the intra-dimer O···O contact, at 3.751(4) Å, is much larger than twice the sum of the van der waals radius of O (3.04 Å). The nature of these intra-dimer contacts afford a slightly 'wedge-shaped' dimer. The angle between the two DTDA planes within the dimer is ~5.6(2)°. The dimers of **1** adopts a π-stacked structure along the *a*-axis (Figure 1a) in which the inter-dimer S···S contacts (4.156(2)–4.180(2) Å) are markedly longer than the intra-dimer S···S distances, like many π-stacked DTDA radicals.[6,13,24-26] Conversely the inter-dimer O···O distance of 3.615(4) Å is comparable with the intra-dimer contact (3.751(4) Å). Each molecule within a dimer forms close contacts to two neighbouring molecules perpendicular to the stacking direction through electrostatically favorable $^{\delta+}$S···N$^{\delta-}$ contacts of the SN-IV type (Scheme 1),[9] leading to a chain-like motif in the *bc*-plane (Figure 1b).

Crystal structures of 2α, 3 and 4

Radicals **2α, 3** and **4** crystallize as c*is-oid* dimers in the space group $P2_1/c$, each with two molecules (one dimer) in the asymmetric unit (Fig. 2; Figs. S1 and S2, ESI). The torsion angles between heterocyclic and perfluoroaryl rings in **2α, 3** and **4** span the range 29.2 – 44.4(2)°, comparable with **1** and other perfluoroaryl DTDAs (*vide supra*).[16,17,23]

Although the intra-dimer S···S contacts (3.049(1) – 3.206(1) Å) remain in the typical range for DTDA radicals (Table 2), the intra-dimer O···O separation increases steadily with increasing chain length from 3.751(4) to 5.379(2) Å, revealing a linear relationship between the length of the alkoxy group and O···O separation (Fig. S3 (left), ESI). This increasing O···O separation reflects additional strain through 'hinging' at the intra-dimer DTDA S...S contacts with the angle between DTDA ring planes increasing form 5.6(2) to 13.3(5)° (Table 2).

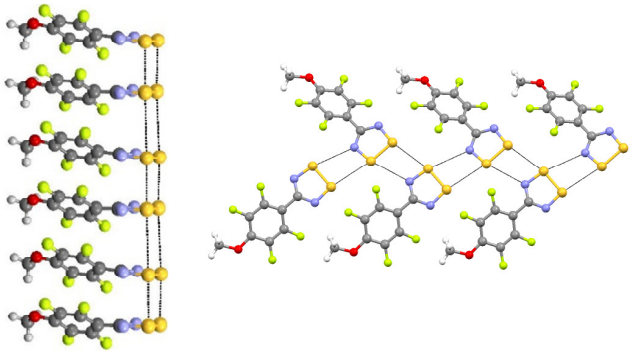

(a) (b)

Figure 1: The crystal structure of **1**. (a) π-stacking parallel to the crystallographic *a*-axis; (b) Propagation of inter-stack contacts *via* SN-IV type interactions in the *bc*-plane.

A consequence of this increased 'wedging' of the dimer geometry is to generate a fundamental change in the π-stacking. While **1**, **2α**, **3** and **4** all crystallise in the $P2_1/c$ space group, the inversion center is located between stacks in **1** (affording an AA'AA' π-stacking motif) but is positioned within stacks in **2α**, **3** and **4**, generating an AA'BB' packing. The latter appears better able to accommodate the more 'wedge-shaped' dimers associated with **2α**, **3** and **4**. The structure of **2α** is shown in Fig. 2. Perpendicular to the stacking direction **2α**, **3** and **4** form similar inter-stack contacts to **1** (compare Fig. 1b and Fig 2b).

Table 2: Selected structural parameters for dimers of **1 – 4**

	Intradimer $d_{S\cdots S}$ (Å)	Intradimer $d_{O\cdots O}$ (Å)	Angle between C_6F_4 and DTDA ring planes (°)	Angle between DTDA ring planes (°)	In plane S···N contacts (Å)	In plane S···F contacts (Å)
1	3.179(2)-3.198(2) mean: 3.188	3.751(4)	30.8(5)-31.2(5) mean: 31.0	5.6(2)	3.295(3)-3.387(3)	3.018(2)-3.232(2)
2α	3.066(2)-3.090(2) mean: 3.078	4.198(4)	29.2(7)-35.3(7) mean: 32.2	8.7(3)	3.102(4)-3.235(4)	2.990(3)-3.235(3)
2β	3.162(8)-3.204(9) mean: 3.183	4.087(4)-4.204(2) mean: 4.145	27(3)-39(3) mean: 33	8.7(4)	3.139(2)-3.372(2)	3.023(9)-3.220(9)
2γ	3.124(6)-3.177(6) mean: 3.150	3.877(2)-4.056(2) mean: 3.966	30(2)-36(2) mean: 33	6.3(2)	2.964(3)-3.324(3)	2.82(3)-3.17(3)
3	3.077(1)-3.137(1) mean: 3.107	4.460(3)	40.0(3)-35.1(3) mean: 37.5	10.0(6)	3.095(2)-3.247(2)	3.091(1)-3.189(1)
4	3.099(1)-3.049(1) mean: 3.074	5.379(2)	44.4(2)-35.2(2) mean: 39.7	13.3(5)	2.998(1)-3.236(1)	3.021(1)-3.200(1)

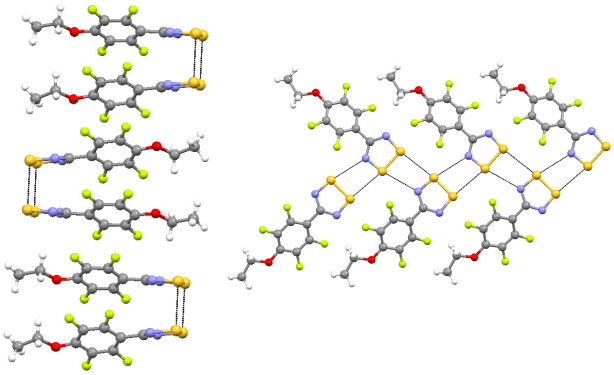

(a) (b)

Figure 2: The crystal structure of **2α** (a) Antiparallel arrangement of dimers parallel to the crystallographic *a* axis; (b) Propagation of inter-stack contacts *via* SN-IV type interactions in the *bc*-plane.

In all cases the in-plane S···N contacts are supplemented by S···F contacts linking dimers together in the *bc* plane. These fall in the range 2.82 – 3.26 Å (Table 2), *cf* sum of the van der Waals radii of S and F (3.27 Å).

Crystals of **2β** were collected at +30 °C but underwent a phase transition below -25 °C to form **2γ** upon cooling, confirmed by DSC measurements (ESI, Fig. S6). Both **2β** and **2γ** showed a propensity for twinning and cooling through the phase transition led to significant degradation in crystal quality. The structures described here are the best of multiple crystals examined.

Crystal structure of 2β

At -20 °C a crystal of **2β** was indexed on a triclinic cell (*P*-1) with 6 molecules in the asymmetric unit. These 6 crystallographically independent molecules comprise two *cis-oid* dimers and two monomeric radicals. The heterocyclic ring planes of the monomers are markedly twisted with respect to the dimer DTDA ring planes (Fig. 3). Structures of DTDA radicals comprising mixtures of both dimers and monomers are rare but not without precedent.[12,14,27] The intra-dimer S···S contacts fall in the range 3.162(8) – 3.204(9) Å (Table 2), while the corresponding intra-dimer O···O separations are 4.087(4) and 4.204(2) Å, comparable with **2α** (4.198(4) Å). The hinge angles between DTDA rings within these dimers are in range 27 – 39 °.

As with other structures in this series, **2β** adopts a π-stacked structure parallel to the crystallographic *b*-axis. The two dimers and two monomers in the asymmetric unit form two crystallographically independent stacks with each stack containing one dimer and one monomer (Fig. 3a). Although the perfluoroaryl rings associated with the two monomeric radicals are well-located, their DTDA rings appears thermally disordered (*vide infra*) *via* rotation of the CNSSN ring about the C_{Ar}-C_{DTDA} bond. In each case this ring was modelled over two orientations. This disorder reveals that there is adequate space between dimers along the stacking direction to accommodate significant DTDA ring rotation in this structure. Notably the major component of disorder in both independent monomers (60% and 85%) reveal the DTDA ring is close to perpendicular to the DTDA rings in the dimers (Fig. 3a). This behaviour is reminiscent of (*o*-$ClC_6H_4CNSSN)_2$ although the latter shows no structural disorder.[27b] Notably the inter-stack contacts still adopt a similar motif to that observed in the other structures in this series (Fig. 3b). In **2β** rotation of 33% of the DTDA rings leads to a mixture of SN-I (two S···N contacts with coplanarity unnecessary) and SN-IV (S···N and S···S contacts between near coplanar DTDA heterocycles). Although the closest centroid…centroid distances between monomers along the stacking direction is 12.4 Å, the two independent rotationally disordered radicals are located adjacent to each other in neighbouring stacks offering an orthogonal π–π interaction between DTDA rings (Fig. 3b). The closest S···S contacts in this arrangement are in excess of 3.8 Å, consistent with a van der Waals interaction rather than a π–π interaction between SOMOs.

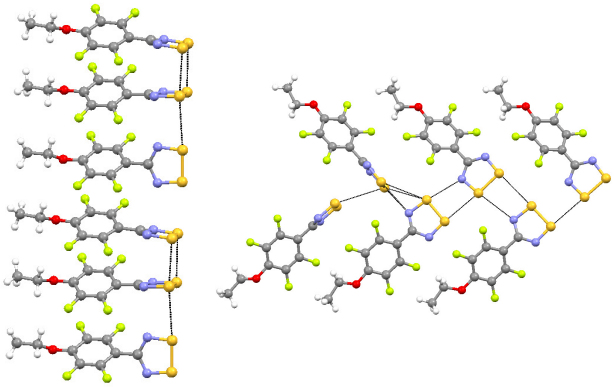

(a) (b)

Figure 3: The crystal structure of **2β**. (a) One of the two crystallographically independent stacks of dimers and monomers in **2β**. (b) Propagation of inter-stack contacts *via* SN-IV and SN-I type interactions.

Crystal structure of 2γ

On cooling below -25 °C, **2β** undergoes a reversible phase transition to **2γ** which is evident in variable temperature powder X-ray diffraction (VT-PXRD) and DSC studies (*vide infra*). Although samples cooled through the phase transition retained crystallinity, the diffraction pattern persistently reflected some degree of twinning in all crystals examined and was reflected in a poorer internal R value (R_{int}) compared to the high temperature phase (Table 1). The emergence of new reflections was consistent with the formation of a super-cell. An examination of the unit cell parameters for **2β** and **2γ** reveal similar *a* and *c* parameters but an increase in the crystallographic *b*-axis from 11.9249(12) to 25.774(4) Å (Table 1). A full dataset was measured at 173 K (75 K below the phase transition) on a crystal cooled through the phase transition. The new data initially indexed on a higher symmetry monoclinic supercell. Structure solution in the $P2_1$ space group provided an initial solution with Z' = 14 but the refinement stalled at R_1 = 27% with evidence for twinning (systematic observation of $F_o > F_c$ for the most disagreeable reflections). A possible two component twin, close to merohedral was identified but failed to provide a significant improvement in R_1.

When the data were reprocessed in the lower symmetry triclinic setting, a similar solution in *P*-1 (*Z*' = 14) was identified. In this case application of the merohedral twin law (-1 0 0 -1 0 0 0 0 1) led to a marked decrease in R_1 and refinement proceeded smoothly to afford a final R_1 of 13%. Although the R value is high it is in line with the intrinsic quality of the data (R_{int} ~ 9%) and linked to the inherent degradation in crystal quality on passing through the phase transition. Attempts to grow single crystals of this low temperature phase directly by using a low temperature cold finger proved unsuccessful due to the thermodynamic preference to crystallise as the form **2α** at these lower temperatures.

The unit cell parameters of **2γ** are similar to those of **2β** but with an expansion of the crystallographic *b* axis and some modification of the unit cell angles. The structure of **2γ** contains 14 molecules in the asymmetric unit, three of which show a small degree of disorder (< 10%) in the orientation of the DTDA ring. Considering only the major component of the disorder then the low temperature structure comprises 6 *cis-oid* dimers and two monomers which can be split into two crystallographically independent stacks, each containing three dimers and a monomer (Fig. 4a). While many DTDA radicals exhibit large Z' structures,[9b] the current example has the largest Z' value of reported DTDA radicals to date.

(a)

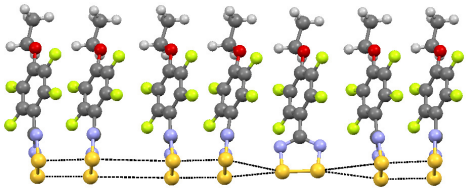

(b)

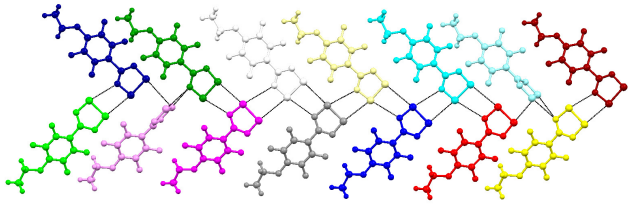

Figure 4: The crystal structure of **2γ**. (a) One of the two crystallographically independent stacks of dimers and monomers; (b) Propagation of inter-stack contacts via SN-IV and SN-I type interactions (molecules coloured by crystallographic independence).

In **2β** the structure comprised an alternating dimer-monomer repeat along the stacking direction (Fig. 3a) whereas **2γ** now exhibits a repeat unit of three dimers and a monomer along the stacking direction (Fig 4a). The combination of the 3 molecule repeat for **2β** and 7 molecule repeat for **2γ** requires a common super-cell containing 21 molecules along the stacking direction. As a consequence, the transition from **2β** to **2γ** not only requires disruption of both the existing dimers but also monomers becoming involved in dimer formation. A representation of the displacement of the radicals in **2β** and **2γ** along the stacking direction in relation to the supercell is presented in Fig. 5. Given the disruption along the stacking direction associated with the phase transition, it is perhaps unsurprising that there was an inherent decrease in crystal quality on passing through this phase transition. As with **2β**, the monomeric radicals in **2γ** exhibit some rotational disorder although this is much reduced when compared to **2β**. In **2γ** monomers are not only well isolated along the stacking direction (monomer…monomer separation ~ 28 Å) but also between stacks (monomer…monomer separation ~13 Å). Between stacks the radicals are once again linked *via* a combination of SN-I and SN-IV type contacts (Fig. 4b).

2β

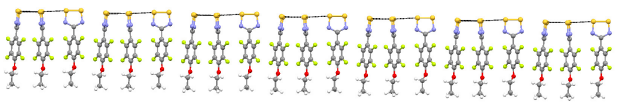

2γ

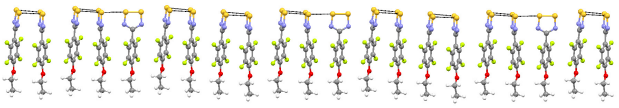

Figure 5: Comparison of the common supercell associated with π-stacking in **2β** (top) and **2γ** (bottom)

Comparison of structures of 1 – 4

DTDA radicals bearing simple phenyl ring substituents often adopt herringbone motifs through $^{\delta+}$S…π interactions as exemplified by $(PhCNSSN)_2$.[28] The inclusion of the perfluoroaryl group reduces π-spin density evidenced by Haynes' charge density studies on $(PhCNSSN)_2$, and $(C_6F_5CNSSN)_2$,[29] suppressing herringbone motifs in these perfluoro-aryl DTDAs.[16-19,23] Their heavier Se analogues[30] also tend to adopt π-stacked/layer-like structures. The structures of **1** – **4** all comprise *layer-like* architectures which maximize inter-stack S···N contacts of the type SN-I and SN-IV (Figs. 1b, 2b, 3b, 4b and ESI. Figs. S1b, S2b). The arrangement of molecules along the stacking direction appears sensitive to the functional group size. While compounds **1**, **2β** and **2γ** adopt π-stacked structures (of the AA'AA' variety), **2α**, **3** and **4** adopt layered structures in which discrete dimers align antiparallel adopting an AA'BB' motif. The former appears stabilized through dispersion and weak inter-dimer bonding interactions whereas the latter is stabilized through dipole-dipole interactions. The increase of the alkyl chain length affords a linear increase of the unit cell volume (Fig. S4 (right)) and a monotonic increase in O···O separation within dimers, affording a more 'wedge-shaped' motif for larger alkyl groups. This subtle change in geometry of the *cis-oid* dimers leads to marked changes in the solid-state packing. While the smaller methoxy derivative **1** forms a π-stacked structure, the larger alkoxy derivatives (**3** and **4**) which exhibit more wedge-shaped geometries adopt AA'BB' motifs as a more efficient packing mode (Fig 6). In the case of **2** there is a fine balance between these two scenarios with polymorphs **2β** and **2γ** exhibiting the AA'AA' motif and **2α** revealing an AA'BB' stacking pattern. In **2β** and **2γ** the AA'AA' packing of the wedge-shaped motif leads to some degree of inefficient packing. At low temperature (**2γ**)

there is just one monomer observed for every three dimers but thermal expansion of the lattice leads to additional monomers at elevated temperatures (**2β** exhibits one monomer for each dimer) enhancing the number of paramagnetic centers in the lattice on warming.

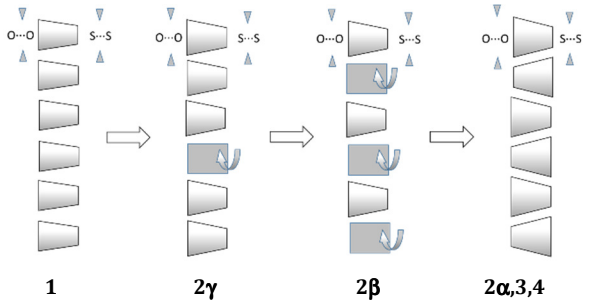

Figure 6: Packing arrangements for **1** – **4**. Trapezoids represent dimers and rectangles represent rotationally disordered monomers.

Thermal studies on 1 – 4

A summary of the thermodynamic data determined from DSC studies for **1 – 4** is presented in Table S2 and values quoted in the text refer to onset temperatures (T_{onset}). DSC studies on **1** and **4** revealed the presence of a single endothermic process at 78 °C and 58 °C for **1** and **4** respectively associated with their melting points. The absence of any additional features on thermal cycling coupled with VT-PXRD studies (see ESI) showed no evidence for polymorphism in these two materials.

The selective preparation of both polymorphs **2α** and **2β** permitted a series of studies on the relative stabilities and phase transitions of **2**. For **2α** variable temperature single crystal and powder X-ray diffraction studies showed no significant structural change in **2α** from -170 to +65 °C (Fig. 7a). At 75(2) °C PXRD studies revealed **2α** had converted to **2β** (Fig. 6). DSC studies on a pure sample of **2α** revealed the presence of two successive endothermic transitions on warming at +76 and +80 °C with a total enthalpy change of ΔH = +20 kJ·mol^{-1} on the heating cycle (ESI, Fig. S6). The first transition is attributed to the conversion of **2α** to **2β** whereas the second is attributed to the melt of **2β.** Upon slow cooling, recrystallization of liquid **2** occurs with formation of **2β**, confirmed by VT-PXRD studies (Fig. 7). A comparison of the structures of **2α** and **2β** reveal that the transformation of **2α** to **2β** requires a major lattice reorganisation (50% of molecules to undergo a 180° rotation or 100% of molecules to undergo a 90° rotation). Previous studies have identified such major lattice reorganizations occur *via* a melt/recrystallization process.[15]

The endothermic nature of the conversion of **2α** to **2β** indicates this spontaneous process is entropically driven such that **2α** is the enthalpically preferred of the two polymorphs and **2β** is the entropically more stable phase. Based on the density rule,[31] (**2α** = 1.842 g·cm^{-3} *cf* **2β** = 1.781 g·cm^{-3}) the lattice enthalpy of **2α** is greater than **2β** in agreement with these experimental observations. DSC studies on a pure sample of **2β** heated from -60 to +150 °C revealed two endothermic transitions occurring at -25 °C and +78 °C. The transition at -25 °C is associated with the phase transition from the low temperature phase **2γ** to the high temperature phase **2β**, corroborated by single crystal and PXRD studies (Fig. 8). The enthalpy change associated with this process (+0.6 kJ·mol^{-1}) is extremely small. The transition at +78 °C (ΔH_{fus} = +19.2 kJ·mol^{-1}) is assigned to

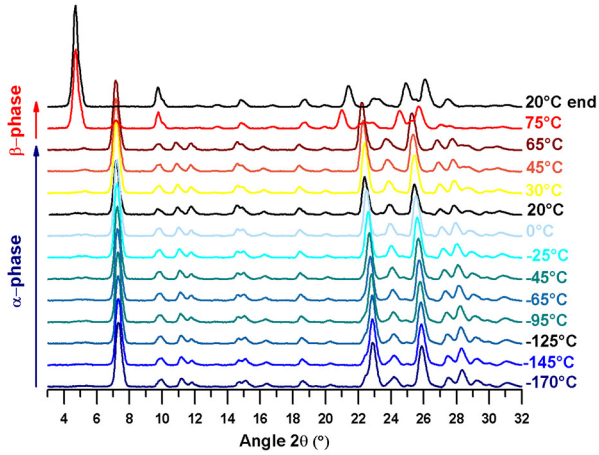

Figure 7: Variable temperature PXRD profiles observed on heating **2α.**

the melting of **2β**. On cooling a small transition at -30 °C was recorded reflecting the reversible nature of the **2γ** to **2β** transition. This behaviour was confirmed by VT-PXRD studies (Fig. 8) which revealed the disappearance of weak peaks around 7° and 16° as well as a more intense feature near 22°/2θ on cooling to -25 °C. More subtle changes in peak position and intensities were evident on cooling from -25 °C to – 170 °C, suggestive of a dynamic process in this regime. In addition the re-emergence of the original PXRD profile on warming back to room temperature confirmed the reversible nature of the **2β** ↔ **2γ** transition seen in DSC studies. Powder patterns for **2β** and **2γ** were in good agreement with those predicted from the single crystal X-ray data.

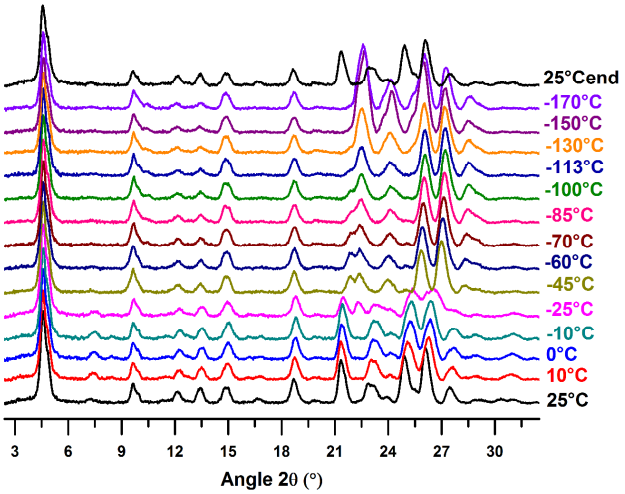

Figure 8: Variable temperature PXRD profiles of **2β** on cooling, converting to **2γ** at -25 °C and subsequent conversion back to **2β** on warming to room temperature.

Application of the density rule (**2β** = 1.781 g.cm^{-3}, *cf* **2γ** = 1.821 g.cm^{-3}) suggests that the lattice enthalpy of **2γ** is greater than that of **2β** and therefore the conversion of **2γ** to **2β** on warming is entropically driven, consistent with the increasing number of disordered monomers. In this context, **2β** can be considered as the most entropically favourable phase whereas **2α** is the most enthalpically favourable phase with **2γ** metastable in the low temperature region. This is entirely consistent with experimental observations that sublimation at high temperature ('cold' finger temperature +30 °C) affords selectively the most entropically favourable phase **2β** whereas sublimation using low substrate temperatures (cold finger set to -15 °C) affords the most enthalpically stable phase (**2α**) with **2γ** only isolated through the solid-state transformation **2β** → **2γ** on cooling.

Radical **3** reveals two endothermic transitions on heating (T_{onset} = 64 and 91 °C, Fig. S7). VT-PXRD studies on **3** reveal no significant change in the profile of the powder pattern across the temperature range 20 – 65 °C, agreeing well with that predicted based on the single crystal structure determination (Fig. S9, ESI). At 80 °C, the pattern changed significantly to afford just a few broad low intensity features. We tentatively assign this to the formation of a glassy phase with some degree of structural order (possibly a liquid crystalline phase). The second transition at 91 °C has a much lower enthalpy change (ΔH = 1.54 kJ.mol^{-1}) consistent with the breakdown of the final components of short range ordering and formation of an isotropic liquid. The integrity of the radical over this temperature range was confirmed by the VT-PXRD studies which revealed reformation of crystalline **3** upon cooling (see Fig. S9, ESI).

Magnetic studies on 2

DC magnetic studies on **2α** and **2β** were measured on a Quantum Design SQUID magnetometer. Data for **2α** (69 mg) were measured from 5 to 300 K with the sample sealed in a gelatin capsule with an applied field of 10,000 Oe. The sample of **2β** (47 mg) was mounted in a quartz tube and measured from 150 to 375 K with an applied field of 10,000 Oe. Additional heating and cooling cycles on **2β** (46 mg) mounted in a gelatin capsule were undertaken in applied fields of 500 Oe to probe the solid-state transition between **2β** and **2γ**. Data were corrected for diamagnetism of both the sample and holder.

For **2α**, the value of χT remains approximately constant at 0.003 emu·K·mol^{-1} on warming up to 250 K (Fig 9(top)), consistent with a small number of S = ½ defects in the crystal lattice (0.6%). Above 250 K the susceptibility of **2α** begins to increase. The onset of significant sample paramagnetism in such DTDA dimers has been reported for a number of DTDA radicals and has previously been shown to be consistent with thermal population of a low-lying excited state triplet.[25,26,32] In the current case, modelling the magnetic data to the Bleaney-Bowers model[33] [H = -2JS$_1$·S$_2$] failed to reproduce the sample's magnetic behavior (dashed line in Fig. 9(top)). Alternatively paramagnetism may arise from some degree of dissociation of the dimers to form monomers in the solid state. Similar arguments have been implemented to model the weak paramagnetism observed in the liquid phase of $F_3CCNSSN$.[34] In this context, we applied a simple monomer-dimer equilibrium model (Eqn. 1) based on a two parameter fit (ΔH_{dim} and ΔS_{dim}) which define the percentage monomer present (see ESI-9).

$$(EtOC_6F_4CNSSN)_2 \rightleftharpoons 2\ EtOC_6F_4CNSSN^{\bullet} \qquad \text{(Eqn. 1)}$$

This behaviour is not unreasonable within the context of the recent pair exchange dynamics model proposed for related thiazyl radicals (*vide infra*).[35] This dimer dissociation model assumes that both exchange coupling (i) between the two radicals generated and (ii) to neighbouring radicals is negligible. At low temperature when the equilibrium lies far to the left (Eqn. 1) then the small numbers of monomer pairs generated are well separated from each other. The latter is certainly a good assumption. The assumption that exchange coupling between radical pairs generated by dimer dissociation is negligible should be treated more cautiously, although computed exchange couplings between radicals at/near the sum of the van der Waals radii are typically an order of magnitude or more less (< 10^2 K) than the intra-dimer exchange coupling.[36]

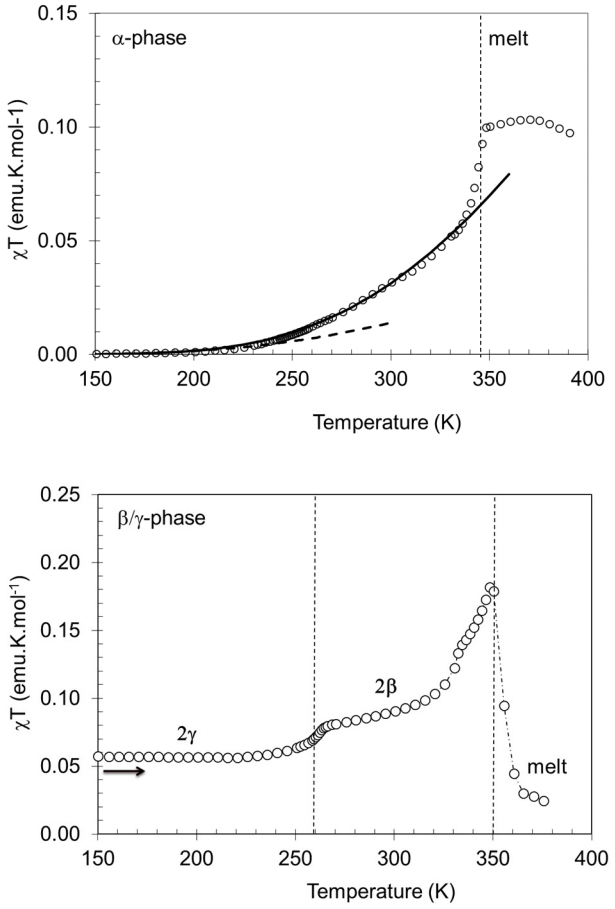

Figure 9: Plots of χT *vs* T for **2α** and **2β/2γ**. For **2α** (top) the dashed line corresponds to the fit to the Bleaney-Bowers model whereas the solid line corresponds to the equilibrium model. For **2β/2γ** (bottom) the vertical dashed line at 259 K corresponds to the maximum observed in the heat capacity and the vertical dashed line at 350 K corresponds to the melting point. The dashed line through the data merely acts as a guide to the eye.

Neglecting the possibility of radical-radical exchange coupling, the magnetic data of **2α** can be well fitted to the equilibrium model with just two parameters. The values of ΔH_{dim} (-30 kJ·mol^{-1}) and ΔS_{dim} (-71 J·K^{-1}·mol^{-1}) are gratifyingly comparable with experimentally determined ΔH_{dim} and ΔS_{dim} values for $(PhCNSSN)_2$ in solution (ΔH_{dim} = -35 kJ·mol^{-1}, ΔS = -121 J·K^{-1}·mol^{-1}).[10b] A surge in the value of χT commences around 340 K and levels off at 350 K and is associated with the melting of **2α** to form liquid **2**.

For **2β/2γ** the low temperature value of χT remains constant at 0.057 emu·K·mol^{-1} up to 250 K (Fig. 9(bottom)), close to the value expected for 1-in-7 radicals being unpaired (0.054 emu·K·mol^{-1}), consistent with the structural data for **2γ**. From 246 to 264 K there is a step in the value of χT, increasing to 0.089 emu·K·mol^{-1}, a little less than that predicted for one third of the molecules contributing to sample paramagnetism (0.125 emu·K·mol^{-1}) anticipated from the structure of **2β**. From 330 to 350 K there is a further increase in paramagnetism up to a maximum of 0.180 emu·K·mol^{-1} as the sample approaches the melting point, corresponding to ca. 50% unpaired spins. This behavior is comparable with other studies on DTDA radicals in the liquid phase where the value of χT remains below the value expected for a pure S = ½ system and has been attributed to aggregation in the melt.[34] The final decrease in χT above the melting point is associated with loss of sample from the cavity space through sublimation and reflected in coating of the quartz sample holder with radical when removed from the magnetometer. Additional studies of the phase transition **2β** ↔ **2γ** in heating and cooling modes confirm the reversible nature of the transition and presence of a small thermal hysteresis loop. If the onset temperatures for the phase transition on heating/cooling are considered then there is negligible hysteresis (T_C = 257(1) K) but if the transition temperatures are defined by the maximum change in gradient of χT(T) then this affords ($T_{C(\uparrow)}$ = 261(1) K, $T_{C(\downarrow)}$ = 256(1) K (scan rate = 1 K·min^{-1})(Fig. 10). Additional heat capacity measurements (scan rate =0.1 K·min^{-1}) agree well with the SQUID data, affording a peak maximum at 259 K.

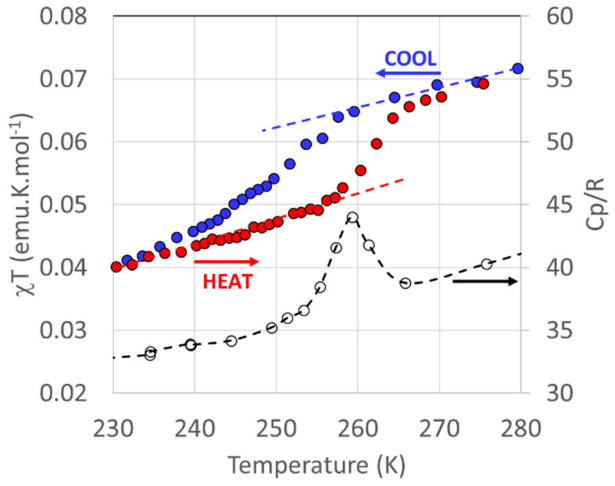

Figure 10: Plot of χT *vs* T on heating and cooling for **2β/2γ** and the heat capacity measured over the same temperature range. The dashed lines merely act as a guide to the eye.

DISCUSSION

Polymorphism in DTDAs is typically manifested in different modes of dimerization and/or different solid-state packing motifs. Even 'simple' radicals such as HCNSSN[37] and ClCNSSN[8,38] where there is no torsional flexibility have been found to be polymorphic. For example ClCNSSN has been isolated as both *cis-oid* dimers (α and γ-polymorphs) and *twisted* dimers (β, δ and ε-polymorphs) reflecting small energetic differences between *cis-oid* and *twisted* dimer conformations.[8,38] Several examples of structures comprising both monomers and dimers in the solid state have been reported,[12,14] highlighting that their dimerization enthalpies are comparable with other packing forces.

There was no evidence for polymorphism in **1** and **4** based on DSC and VT-PXRD studies. For **3** the variable temperature studies showed some evidence for an intermediate glassy or liquid crystalline phase occurring between the crystalline and liquid phases (64 – 91 °C) but again no direct evidence for additional polymorphs was observed during our thermal studies on this material. The polymorphism in **2** appears to arise as a result of its structurally intermediate nature between **1** (which adopts an AA'AA' stacked structure) and **3** and **4** (which adopt an AA'BB' stacking). The significant structural differences between **2α** and **2β** are reflected in a melt-recrystallisation process for the irreversible endothermic **2α** → **2β** transformation, comparable to the phase transition between α and β phases of *p*-NCC_6F_4CNSSN.[15] The instability in **2β** on cooling cannot be alleviated by a **2β** → **2α** transformation, but adopts an alternative metastable state **2γ** which is more enthalpically favourable than **2β**. The reversible solid-state phase transition between **2β** and **2γ** necessitates a combination of small molecular displacements and ring rotations along the stacking direction (Fig. 5). The differing number of monomers in **2β** (33%) and **2γ** (14%) leads to an associated change in magnetic response. Such single crystal to single crystal phase transitions are not without precedent in thiazyl radical chemistry. In the current case the aryl substituents provide a well-defined framework of near-regular displacements along the stacking direction which are mis-matched with the spin-Peierls driven dimerization of the DTDA groups. This mismatch between regular and irregular displacements appears to support dynamic behaviour along the stacking direction. Similar displacive transitions have been reported within the family of dithiazolyls such as TTTA,[39] PDTA[40] and NCBDTA (Scheme 4).[41]

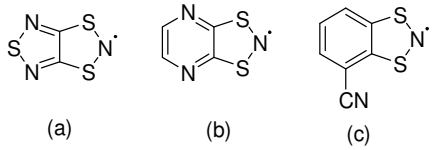

Scheme 4: (a) 1,3,5-trithia-2,4,6-triazapentalenyl (TTTA) (b) 1,3,2-dithiazolo[4,5-*b*]pyrazin-2-yl (PDTA) (c) 3-cyanobenzo-1,3,2-dithiazolyl (NCBDTA)

In the case of TTTA and PDTA these transitions show significant thermal hysteresis associated with the cleavage of inter-stack contacts.[42] *Ab initio* molecular dynamics simulations on TTTA[35] indicate fast intra-stack pair-exchange dynamics in which displacive motion of the radicals along

the stacking direction plays a key role in driving the phase transition.Structural transitions in DTDA chemistry which resemble the **2β** ↔ **2γ** transformation are few.[27a,43] The first order transitions associated with a lanthanide-bridging DTDA complex described by Preuss[11b] comprise two sequential structural phase transitions at 160 and 310K which involve rupture of 50% (160 K) and 100% (310 K) of the DTDA π*-π* dimer interactions.

CONCLUSIONS

The length of the alkoxy chain influences the solid-state structures of the alkoxy-tetrafluorophenyl DTDA radicals **1** – **4** in a systematic fashion. The ethoxy derivative **2** appears to be at the crossing point in terms of structure stability and was found to be polymorphic; **2α** adopts the AA'BB' dimer motif observed for **3** and **4** whereas **2β** and **2γ** adopt a cofacial packing arrangement akin to **1**. Unlike **1**, the structure of **2β** is more complex with the structure seemingly unable to support formation of a pure dimer phase. At low temperature, the structure of **2γ** comprises a 3:1 ratio of dimers to monomers, whereas in the high temperature phase **2β** exhibits a dimer:monomer ratio of 1:1. The rich polymorphism and phase transition behaviour associated with **2** was probed by DSC, VT-PXRD and SQUID magnetometry. These reveal an irreversible transition from **2α** to **2β** upon warming and a reversible transition between the high temperature phase **2β** and the low temperature form (**2γ**) which are associated with a unique dynamic process along the stacking direction involving both displacive and rotational motion of the DTDA radicals.

ASSOCIATED CONTENT

Supporting Information

Experimental details of the preparation of the starting nitriles, ROC_6F_4CN, and radicals **1** – **4**; Crystallographic details of the data collection, processing and refinement for **1** – **4**; DSC studies on **1** – **4**; VT-PXRD studies on **3**; Computations of the exchange coupling in dimers of **1** – **4**; Details of the magnetic measurements on **2**. The Supporting Information is available free of charge on the ACS Publications website at DOI: xxxxxxx Crystal structures of **1** – **4** including variable temperature structural studies on **2α** (103–268 K) in cif format.

AUTHOR INFORMATION

Corresponding Author

* jmrawson@uwindsor.ca

Present Addresses

† R. Sun, Department of Chemistry and Chemical Biology, Harvard University, 12 Oxford Street, Cambridge, MA 02138, United States.

Author Contributions

Synthetic work was carried out by Y.B., R.S. and R.J.L.; magnetic measurements were made by A.A. and J.C. Structural studies and magnetic analysis by Y.B. and J.M.R. Manuscript drafted by Y.B. and J.M.R. with additional contributions from all authors. All authors have given approval to the final version of the manuscript.

Notes

The structure of **1** – **4** have been deposited with the CCDC (deposition numbers 1565879 – 1565888).

ACKNOWLEDGMENT

We would like to thank the Canada Research Chairs Program for financial support (J.M.R.), the University of Windsor for a scholarship (Y.B.) and C.F.I./O.R.F. support for infrastructure. We thank the Inorganic Chemistry Exchange (I.C.E.) Program for the opportunity for R.S. to visit U. Windsor. We also acknowledge support from the Ministerio de Economía y Competividad of Spain (Grant No. MAT2015-68200- C2-2-P). Additional support from Diputación General de Aragón (DGA-M4) is also acknowledged. (J.C. and A.A)

REFERENCES

(1) Bryan, C. D.; Fleming, R. M.; Glarum, S. H.; Haddon, R. C.; Oakley, R. T.; Palstra, T. T. M.; Perel, A. S.; Schneemeyer, L. F.; Waszczak, J. V.; Cordes, A. W. *Nature* **1993**, *365*, 821.

(2) Thomson, R. I.; Pask, C. M.; Lloyd, G. O.; Mito, M.; Rawson, J. M. *Chem. Eur. J.* **2012**, *18*, 8629.

(3) Iwasaki, A.; Hu, L.; Suizu, R.; Nomura, K.; Yoshikawa, H.; Awaga, K.; Noda, Y.; Kanai, K.; Ouchi, Y.; Seki, K.; Ito, H. *Angew. Chem. Int. Ed. Engl.* **2009**, *48*, 4022.

(4) (*a*) Preuss, K. E. *Dalton Trans.* **2007**, 2357. (*b*) Preuss, K. E. *Coord. Chem. Rev.* **2015**, *289*, 45. (b) Lau, H. F.; Ng, V. W. L.; Koh, L. L.; Tan, G. K.; Goh, L. Y.; Roemmele, T. L.; Seagrave, S. D.; Boeré, R. T. *Angew.Chem.,Int.Ed.* **2006**, *45*, 4498.

(5) (a) Banister, A. J.; May, I.; Rawson, J. M.; Smith, J. N. B. *J. Organomet. Chem.* **1998**, *550*, 241. (b) Banister, A. J.; Gorrell, I. B.; Clegg, W.; Jørgensen, K. A. *J. Chem. Soc. Dalton Trans.* **1989**, 2229.

(6) (a) Beldjoudi, Y.; Osorio-Roman, I.; Nascimento, V.; Rawson, J. M.; *J. Mater. Chem.C.* **2017**, *5*, 2794. (b) Beldjoudi, Y. PhD Thesis, University of Windsor, **2016**.

(7) Rawson, J. M.; Alberola, A.; Whalley, A. *J. Mater. Chem.* **2006**, *16*, 2560.

(8) Bond, A.D.; Haynes, D. A.; Pask , C.M.; Rawson, J. M. *J. Chem. Soc., Dalton Trans.* **2002**, 2522.

(9) (a) Haynes, D. A. *CrystEngComm*, **2011**, *13*, 4793; (b) R.T. Boeré and N.D.D. Hill, *CrystEngComm*, **2017**, *19*, 3698.

(10) (a) Brooks, W.V.F.; Burford, N.; Passmore, J.; Schriver, M.J.; Sutcliffe, L.H. *J.C.S. Chem. Commun.* **1987**, 69 ; (b) Fairhurst, S. A. ; Johnson, K. M. ; Sutcliffe, L. H.; Preston, K. F. ; Banister, A. J. ; Hauptman, Z.V. ; Passmore, J. *J. Chem. Soc. Dalton Trans.*, **1986**, 1465.

(11) (a) Fatila, E. M.; Maahs, A. C.; Mills, M. B.; Rouzières, M.; Soldatov, D. V.; Clérac, R.; Preuss, K. E.; *Chem. Commun.* **2016**, *52*, 5414. (b) Fatila, E. M.; Mayo, R. A.; Rouzières, M.; Jennings, M. C.; Dechambenoit, P.; Soldatov, D. V.; Mathonière, C.; Clérac, R.; Coulon, C.; Preuss, K. E. *Chem. Mater.* **2015**, *27*, 4023.

(12) Alberola, A.; Clarke, C. S.; Haynes, D. A.; Pascu, S. I.; Rawson, J. M. *Chem. Commun.* **2005**, 4726.

(13) Clarke, C. S.; Haynes, D. A.; Smith, J. N. B.; Batsanov, A. S.; Howard, J. A. K.; Pascu, S. I.; Rawson, J. M. *CrystEngComm,* **2010**, *12*, 172.

(14) Fatila, E. M.; Jennings, M. C.; Goodreid, J.; Preuss, K. E. *Acta Cryst. C* **2010**, *66*, 260.

(15) Beldjoudi, Y.; Arauzo, A.; Palacio, F.; Pilkington, M.; Rawson, J. M. *J. Am. Chem. Soc.,* **2016**, *138,* 16779.

(16) (a) Banister, A. J.; Bricklebank, N.; Clegg, W.; Elsegood, M. R. J.; Gregory, C. I.; Lavender, I.; Rawson, J. M.; Tanner, B. K. *J. Chem. Soc., Chem. Commun.* **1995**, 679. (b) Banister, A. J.; Bricklebank, N.;

Lavender, I.; Rawson, J. M.; Gregory, C. I.; Tanner, B. K.; Clegg, W.; Elsegood, M. R. J.; Palacio, F. *Angew. Chem., Int. Ed.,* **1996**, *35*, 2533.
(17) Alberola, A.; Less, R. J.; Palacio, F.; Pask, C. M.; Rawson, J. M. *Molecules* **2004**, *9*, 771.
(18) Alberola, A.; Less, R. J.; Pask, C. M.; Rawson, J. M.; Palacio, F.; Oliete, P.; Paulsen, C.; Yamaguchi, A.; Farley, R. D.; Murphy, D. M. *Angew. Chem., Int. Ed.* **2003**, *42*, 4782.
(19) Antorrena, G.; Davies, J. E.; Hartley, M.; Palacio, F.; Rawson, J. M.; Smith, J. N. B.; Steiner, A. *Chem. Commun.* **1999**, 1393.
(20) (a) Kyoichi, T.; Hideki, S.; Patent No JP 06145129, May 24, **1994**. (b) Birchall, J. M. ; Haszeldine, R. N.; Jones, M. E. *J. Chem. Soc. C*, **1971**, 1343.
(21) Robinson, S. W.; Haynes, D. A.; Rawson, J.M. *CrystEngComm*, **2013**, 15, 10205.
(22) (a) Boeré, R. T. *CrystEngComm*, **2016**, *18*, 2748; (b) Mills, M. B.; Hollingshead, A. G.; Maahs, A. C.; Soldatov, D. V.; Preuss, K. E. *CrystEngComm*. **2015**, *17*, 7816.
(23) (a) Allan, C.; Haynes, D. A.; Pask, C. M.; Rawson, J. M.; *CrystEngComm*. **2009**, *11*, 2048. (b) Domagała, S.; Haynes, D. A.; *CrystEngComm*. **2016**, *18*, 7116.
(24) (a) Banister, A. J.; Batsanov, A. S.; Dawe, O. G.; Herbertson, P. L.; Howard, J. A. K.; Lynn, S.; May, I.; Smith, J. N. B.; Rawson, J. M.; Rogers, T. E.; Tanner, B. K.; Antorrena, G.; Palacio, F. *J. Chem. Soc. Dalton Trans.* **1997**, 2539. (c) Bell, A. M. T.; Smith, J. N. B.; Attfield, J. P.; Rawson, J. M.; Shankland, K.; David, W. I. F. *New J. Chem.* **1999**, 23, 565.
(25) (a) Constantinides, C. P.; Eisler, D. J.; Alberola, A.; Carter, E.; Murphy, D. M.; Rawson, J. M. *CrystEngComm.* **2014**, *16*, 7298.
(26) Constantinides, C. P.; Carter, E.; Eisler, D.; Beldjoudi, Y.; Murphy, D. M.; Rawson, J. M. *Cryst. Growth Des.* **2017**, *17*, 3017.
(27) (a) Barclay, T. M.; Cordes, A. W.; George, N. A.; Haddn, R. C.; Itkis, M. E.; Oakley, R. T.; *Chem.Comm.*, **1999**, 2269; (b) Alberola, A.; Carter, E.; Constantinides, C. P.; Eisler, D. J.; Murphy, D. M.; Rawson, J. M. *Chem.Comm.* **2011**, *47*, 2532.
(28) Vegas, A.; Pérez-Salazar, A.; Banister, A. J.; Hey, R. G. *J. Chem. Soc., Dalton Trans.* **1980**, 1812.
(29) Domagała, S.; Kosc, K.; Robinson, S. W.; Haynes, D. A.; Woźniak, K. *Cryst. Growth Des.* **2014**, *14*, 4834.
(30) (a) Feeder, N.; Less, R. J.; Rawson, J. M.; Oliete, P.; Palacio, F. *Chem.Commun.* **2000**, 2449; (b) Melen, R. L.; Less, R. J.; Pask, C. M.; Rawson, J. M. *Inorg. Chem.*, **2016**, *55*, 11747.
(31) (a) Burger, A.; Ramberger, R. *Mikrochim Acta.* **1979**, *2*, 273. (b) Burger, A.; Ramberger, R. *Mikrochim. Acta.* **1979**, *2*, 259.
(32) Shuvaev, K. V.; Decken, A.; Grein, F.; Abedin, T. S. M.; Thompson, L. K. ; Passmore, J. *Dalton Trans.* **2008**, 4029.
(33) Bleaney, B.; Bowers, K.D. *Proc. R. Soc. A* **1952**, *214*, 451.
(34) Du, H.; Haddon, R. C.; Krossing, I.; Passmore, J.; Rawson, J.M.; Schriver, M J., *Chem.Comm..*, **2002**, 1836.
(35) Vela, S.; Mota, F.; Deumal, M.; Suizu, R.; Shuku, Y.; Mizuno, A.; Awaga, K.; Shiga, M.; Novoa, J. J.; Ribas-Arino, J. *Nat. Commun.* **2014**, *5*, 4411.
(36) Luzon, J.; Campo, J.; Palacio, F.; McIntyre, G. J.; Rawson, J.M. *Polyhedron*, **2005**, *24*, 2579; (b) Deumal, M.; Rawson, J. M.; Goeta, A. E.; Howard, J. A. K.; Copley, R. C.; Robb, M. A.; Novoa, J. J. *Chem. Eur. J.*, **2010**, *16*, 2741.
(37) (a) Bryan, C. D.; Cordes, A. W.; Haddon, R. C.; Hicks, R. G.; Kennepohl, D. K.; MacKinnon, C.D.; Oakley, R. T.; Palstra, T. T. M.; Perel, A. S.; Scott, S. R.; Schneemeyer, L. F.; Waszczak, J. V. *J. Am. Chem. Soc.*, **1994**, *116*, 1205. (b) Cordes, A. W.; Bryan, C. D.; Davis, W. M.; de Laat, R. H.; Glarum, S. H.; Goddard, J. D.; Haddon, R. C.; Hicks, R. G.; Kennepohl, D. K.; Oakley, R. T.; Scott, S. R.; Westwood, N. P. C. *J. Am. Chem. Soc.,* **1993**, *115*, 7232.
(38) (a) Knapp, C.; Lork, E.; Gupta, K.; Mews, R.; *Z. Anorg. Allg. Chem.*, **2005**, *631*, 1640; (b) Clarke, C. S.; Pascu, S. I.; Rawson, J.M. *CrystEngComm.*, **2004**, *6*, 79.
(39) Fujita, W.; Awaga, K. *Science* **1999**, *286*, 261.
(40) Brusso, J. L.; Clements, O. P.; Haddon, R. C.; Itkis, M. E.; Leitch, A. A.; Oakley, R. T.; Reed, R. W.; Richardson, J. F. *J. Am. Chem. Soc.*, **2004**, *126,* 14692.
(41) Alberola, A.; Collis, R. J.; Humphrey, S. M.; Less, R. J.; Rawson, J.M.; 2006. *Inorg chem*. **2006**, *45*, 1903.
(42) Clarke, C. S.; Jornet-Somoza, J.; Mota, F.; Novoa, J. J.; Deumal, M. *J. Am. Chem. Soc.* **2010**, *132*, 17817.
(43) Suizu, R.; Iwasaki, A.; Shuku, Y.; Awaga, K. *J.Mat.Chem.C*, **2015**, *3*, 7968.

For Table of Contents Use Only

Structural variations in the dithiadiazolyl radicals *p*-ROC$_6$F$_4$CNSSN (R = Me, Et, ^{n}Pr, ^{n}Bu): A case study of reversible and irreversible phase transitions in *p*-EtOC$_6$F$_4$CNSSN.

Y. Beldjoudi, R. Sun, A. Arauzo, J. Campo, R. J. Less and J. M. Rawson

The radical *p*-EtOC$_6$F$_4$CNSSN is found to exhibit three polymorphs with up to 14 molecules in the asymmetric unit. DSC and PXRD reveal an irreversible transition between **2α** and **2β** upon warming. Conversely polymorph **2γ** only appears accessible from **2β** through a reversible solid-state phase transition which involves both rotational and translational motion.